Communications in Computational Chemistry
Commun. Comput. Chem., Vol. 1, No. 2, 97–103
doi: 10.4208/cicc.2025.70.01
Regular Article

Insights into the Chalcogen Bonding Catalysis on the CO_2 Fixation with Styrene Oxide

Haohao Zhang[1,†], Chang Zhao[1,†], Yanjiang Wang[1], Wen-Kai Chen[1,*] and Yanli Zeng[1,*]

[1] *College of Chemistry and Material Science, Hebei Key Laboratory of Inorganic Nano-materials, Hebei Normal University, Shijiazhuang, 050024, China.*

[*] Corresponding authors: wenkaichen@hebtu.edu.cn; yanlizeng@hebtu.edu.cn

[†]These authors contributed equally to this work.

Received on 11 March 2025; Accepted on 20 April 2025

Abstract: The fixation of CO_2 is a promising carbon-neutral approach and drawing lots of attention in the past decades. Among lots of fixation of CO_2 methods, the cycloaddition of CO_2 into epoxides (CCE) reaction is important because it could generate high value-added products. Recently, employing chalcogen bonding (ChB) catalysts for the CCE reaction has been proposed and offers significant advantages of low price, environmental friendliness, and ease of recycling. In this work, the ChB catalyzed the CCE reaction is investigated by high level theoretical calculations. The reaction can be divided into three sub-processes: ring-opening, nucleophilic addition, and formation of cyclic carbonate. Both Se- and Te-based ChB catalysts have shown the potential for catalyzing the CCE reaction, the overall catalytic performance of Te-based catalysts was superior to the Se-based ones. Overall, the most positive electrostatic potentials of the ChB catalysts, electrostatic term of the ChB binding energies, electron density at the ChB critical points, and electron density difference play important roles in the ChB catalyzed CCE reaction. This work elucidated the ChB catalyzed mechanism of the CCE reaction and provided theoretical guidance for the future development of efficient ChB catalysts for the CCE reaction.

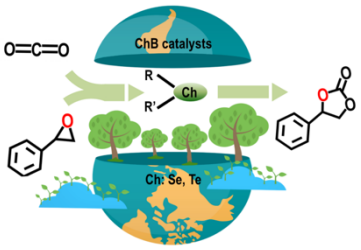

Key words: chalcogen bonding catalysis, CO_2 fixation, density functional theory, QTAIM.

1. Introduction

Non-covalent interactions, such as halogen bonding (XB) [1-3], and chalcogen bonding (ChB) [4-5], have garnered increasing attention in organocatalysis due to their advantages, including non-toxicity, environmental friendliness, broad applicability, low cost, and high reactivity. ChB is defined as the interaction between chalcogen atoms (O, S, Se, or Te) and Lewis bases (LB) [6-7]. Compared to halogen elements, chalcogen elements have stronger positive electrostatic potential regions, characterized by enhanced σ-hole [8] interactions and a greater variety of interaction sites, leading to better catalytic effects. Notably, ChB catalysis as a new catalytic strategy is a more efficient organocatalytic strategy. Matile's group first reported the application of ChB catalysis [9], which has since been applied to a range of reactions, including the Michael addition reaction [10], bromination reaction [11], and Diels-Alder reaction [12], demonstrating excellent catalytic performance. The development of efficient catalysts and the exploration of a broader range of reactions are important in chalcogen bond catalysis.

The fixation of CO_2 into economically high value-added products is one of the most important approaches to achieving

the goal of carbon neutrality [13-15]. Particularly, cyclic carbonate, which is generated by the cycloaddition of CO_2 into epoxides (CCE) reaction, is one of the most important products of the fixation of CO_2 because of their utility in the field of lithium-ion batteries, non-native polar solvents, and fuel additives, etc [16-19]. Moreover, the CCE reaction is capable of achieving 100% atom economy [20, 21], which is in line with the core concept of green chemistry [22-24]. Therefore, exploring a green, eco-friendly, and efficient catalytic method is of great significance. Recently, Kumar and colleagues have reported lots of newly synthesized Te-based catalysts, and a Te-I bond is observed in tellurenyl iodides. However, the prepared tellurenyl iodides could be transformed into another class of organotellurium molecules, namely, ebtellur, owing to the labile nature of the Te-I bond. The Te-N heterocycle ebtellur is identified as an active catalyst in the reaction of CO_2 with epoxides to afford cyclic carbonates (Scheme 1a) [25], the N-Te···O chalcogen bond efficiently catalyzes the reaction, while I^- primarily assists in the ring-opening step. However, the mechanistic details of the CCE reaction remain unraveled.

In this work, inspired by the work of Kumar et al., eight ChB donors as catalysts (Scheme 1b) are employed to catalyze the cycloaddition reaction of CO_2 with styrene oxide. Cat-1, Cat-3, Cat-5, and Cat-7 (the Se-based catalysts) were categorized into one category, whereas Cat-2, Cat-4, Cat-6, and Cat-8 (the Te-based catalysts) were categorized into a separate category. We aim to investigate the mechanism of CO_2 fixation with styrene oxide catalyzed by ChB catalysis, to compare the Se-based and Te-based ChB catalysis, and to explore the designing strategy of the ChB catalysts.

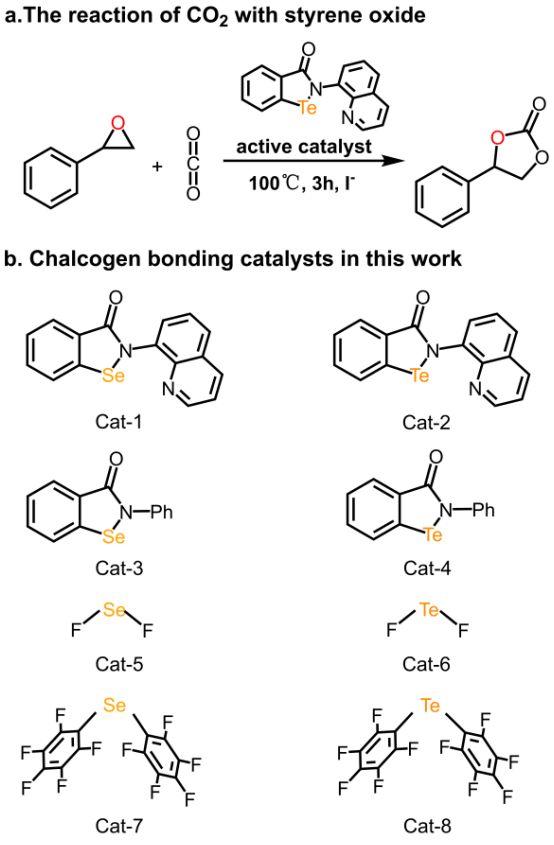

Scheme 1. The chalcogen bonding catalysis on the reaction of CO_2 with styrene oxide.

2. Theoretical method

In this work, the M06-2X-D3/def2-TZVP level of theory was employed for all geometry optimization and electronic structure analysis [26-29]. All geometries, including reactants, catalysts, intermediates, transition states, and products, were optimized using the Gaussian 16 program package [30]. The Conformer-Rotamer Ensemble Sampling Tool (CREST) [31-33] was used for determining the lowest-energy conformers. The low-energy geometries from CREST processes were further optimized with Gaussian 16 to finally determine the lowest-energy conformers. The implicit solvation model is used during all DFT calculations. Styrene oxide solvent was used as the solvent within the IEFPCM solvation model to account for solvent effects [34]. The dielectric constant (ε) of styrene oxide was estimated using the Clausius-Mossotti equation and given as 2.336 [35-36]. Frequency calculations were performed at the same theoretical level to validate the optimized geometries: reactants, catalysts, intermediates, and products exhibited no imaginary frequencies, while transition states displayed only one imaginary frequency. Additionally, intrinsic reaction coordinate (IRC) calculations were conducted to confirm the connectivity of transition states with their corresponding reactants and products [37]. All Gibbs free energies, including translational entropy corrections for the solution phase, were calculated using the THERMO program [38]. The electrostatic potentials (ESPs) [39] of reactants and catalysts were calculated at 0.001 a.u. electron density isosurface. ESP, natural locational molecular orbital (NLMO) [40], and molecular formation density difference (MFDD) analyses [41-43] were performed using the Multiwfn-3.8 [44] and visualized with VMD-1.9.4 [45]. Molecular structures were rendered using CYLview 20 [46]. To quantitatively evaluate the contributions of different factors to the catalytic performance of the ChB catalysts, GKS-EDA was employed to compute intermolecular interaction energies using the modified GAMESS (2020 R2) package at the M06-2X/def2-TZVP level [47-49]. Additionally, topological analysis of electron density at bond critical points (BCPs) was performed using the AIMALL software based on the quantum theory of atoms in molecules (QTAIM) [50-52].

3. Results and discussion

3.1 Electrostatic potential analysis

Electrostatic potential (ESP) analysis has been demonstrated to be an effective method for analyzing and predicting the reactive sites for elucidating the mechanism of weak-interaction catalyzed reactions [53-54]. Therefore, the electrostatic potentials of styrene oxide and eight ChB catalysts were analyzed in this work (Figure 1). For styrene oxide, which will act as a ChB acceptor, the most negative ESP ($V_{s,\,min}$) is located on the area of the O atom in the three-membered ring. On the other hand, for the eight ChB catalysts, the most positive ESP ($V_{s,\,max}$) is found along the axes of the covalent bond chalcogen atom (i.e. Se/Te atom), corresponding to the "σ-hole" region. It can be predicted that the Te/Se atom in ChB catalysts can interact with the O atom in styrene oxide to form ChB. The following discussion will show that these ChB play important roles in the CCE reaction.

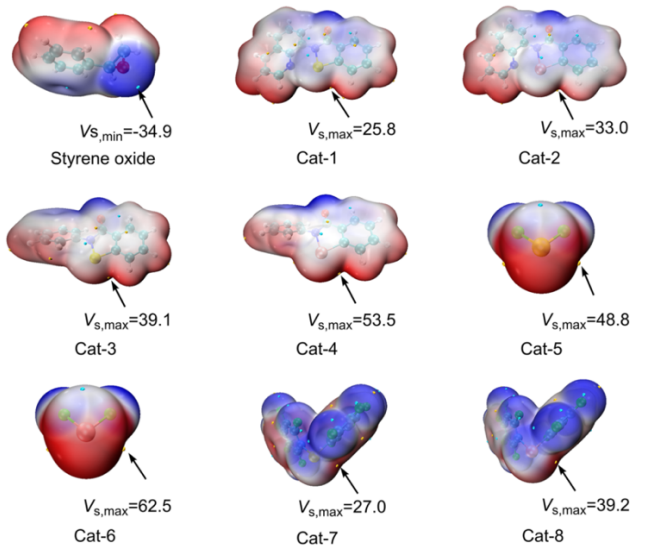

Figure 1. Electrostatic potential maps on the 0.001 a.u. (electrons/bohr^3) contour of the electronic density (kcal/mol) of styrene oxide, Cat-1, Cat-2, Cat-3, Cat-4, Cat-5, Cat-6, Cat-7, and Cat-8.

3.2 Mechanism of the CCE reaction catalyzed by chalcogen bonding catalysts

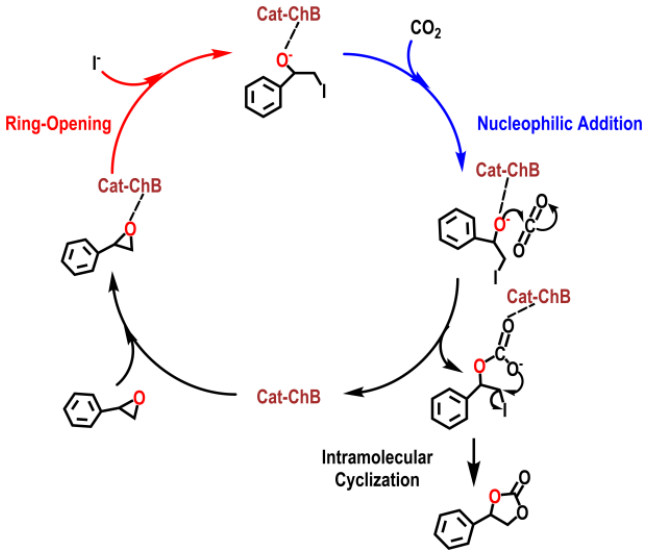

Scheme 2. The catalytic cycle for the CCE reaction catalyzed by ChB catalysts.

Based on previous studies [25], the catalytic cycle for ChB donor catalyzed the cycloaddition reaction of CO_2 with styrene oxide is illustrated in Scheme 2, which can be divided into three steps: (1) ring-opening step, (2) nucleophilic addition step, and (3) intramolecular cyclization step. The Gibbs free energy curves for the cycloaddition reaction of CO_2 with styrene oxide catalyzed by chalcogen bonding catalysts are shown in Figure 2. As Cat-2 is an example, the geometries of the reaction are shown in Figure S1.

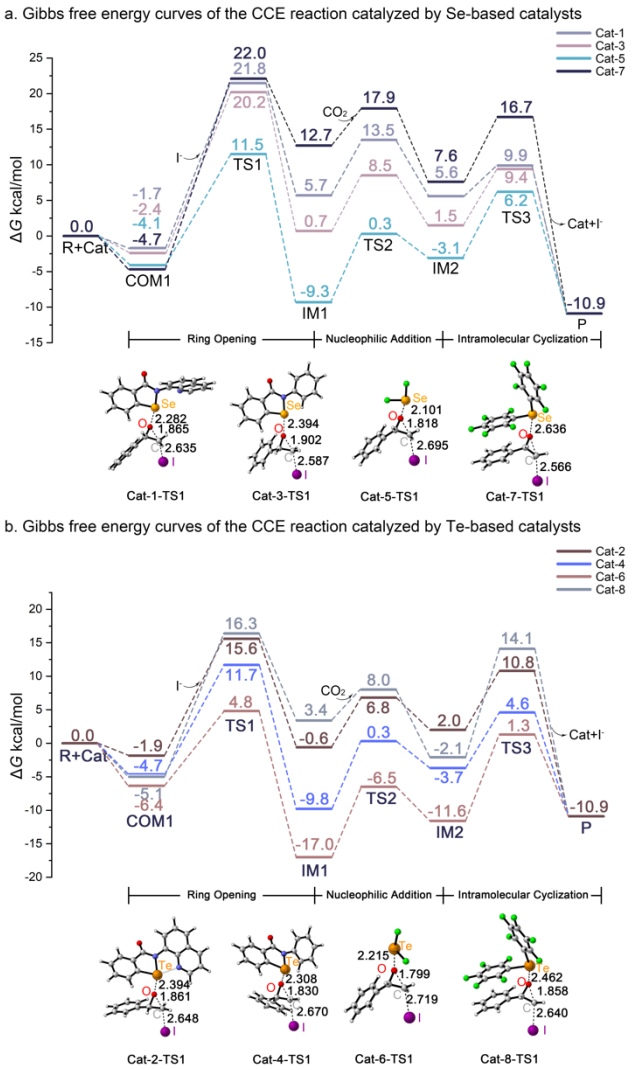

Figure 2. Gibbs free energy curves of the CCE reaction catalyzed by chalcogen bonding catalysts.

(a) Ring-opening step

The ring-opening step consists of the ChB formation between the chalcogen atom in the catalyst and the O atom in styrene oxide and the formation of the C-I bond with the cleavage of the C-O bond. The ChB donor could activate the styrene oxide and generate the initial complex (i.e. Cat-X-COM1, X=1 to 8). The optimized geometries of Cat-X-COM1 and the atomic distances between O and the corresponding chalcogen atom are illustrated in Figure 3. The distances between the Se atom and the O atom in Cat-1-COM1, Cat-3-COM1, Cat-5-COM1, and Cat-7-COM1 are 2.864 Å, 2.817 Å, 2.563 Å, and 3.010 Å, respectively, which are shorter than the sum of the van der Waals radii of Se and O atoms (ca. 3.42 Å) [55]. In Cat-2-COM1, Cat-4-COM1, Cat-6-COM1, and Cat-8-COM1, the distances between the Te atom and the O atom are 2.914 Å, 2.765 Å, 2.601 Å, and 2.957 Å, respectively, which are also shorter than the sum of the van der Waals radii of Te and O atoms (ca. 3.58 Å) [55]. Furthermore, as Cat-X-COM1 (X=1,2) are examples, we performed NLMO analysis as shown in Figure S2. These observations are consistent with the definition of ChB, indicating the formation of a ChB between the catalysts and styrene oxides. The binding energy of COM1s not only correlates with $V_{s,max}$ but also with the kind of

chalcogen atom (Se/Te). As many previous works have reported, the ChBs formed by Te atoms are usually stronger than those of Se atoms [56-57]. The present work is also consistent with this speculation.

Then, after the activation of styrene oxide by the ChB catalysts, the I anion interacts with the C(1) atom, forming a C(1)-I bond with the cleavage of the C(1)-O bond. The free energy barriers of the ring-opening step catalyzed by Cat-1, Cat-2, Cat-3, Cat-4, Cat-5, Cat-6, Cat-7, and Cat-8 are 23.5, 17.5, 22.6, 16.4, 15.6, 11.2, 26.7, and 21.4 kcal/mol respectively, indicating the ring-opening step could happen with the formation of Cat-X-IM1 via the transition state Cat-X-TS1, see Figure 2. Additionally, Cat-5 has the lowest energy barrier among all Se-based catalysts while Cat-6 has the lowest free energy barrier among all Te-based catalysts, which elucidates that the Ch-F_2 (Ch=Se/Te, i.e. Cat-5 and Cat-6) catalysts perform best in all these eight catalysts. In addition, as we have mentioned above, different ChB catalysts with different kinds of chalcogen atoms can also activate styrene oxide and facilitate the ring-opening reaction, and the Te-based catalysts are easier than Se-based ones.

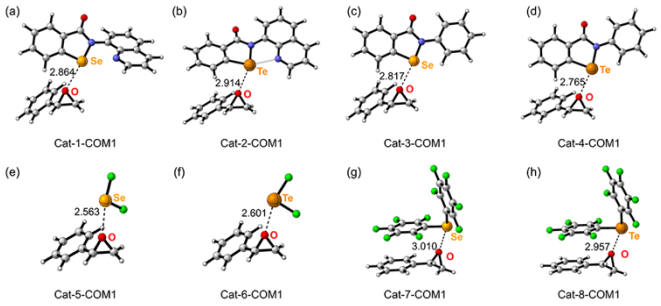

Figure 3. Optimized geometries with the atomic distance between the chalcogen atom and O (in Å) of Cat-X-COM1.

(b) Nucleophilic addition step

The nucleophilic addition step happens after the formation of Cat-X-IM1 through the ring-opening process, in which the nucleophilic O atom of Cat-X-IM1 reacts with the electrophilic C atom of CO_2. During this step, the O atom of styrene oxide is activated by the ChB catalysts, facilitating its nucleophilic addition to CO_2 and leading to the formation of Cat-X-IM2. According to the Gibbs free energy curves (Figure 2), the energy barriers of the nucleophilic addition step are 15.2, 8.7, 10.9, 10.1, 9.6, 10.5, 22.6, and 13.1 kcal/mol, respectively. The catalytic performance of the Te-based catalysts also surpasses that of the Se-based catalysts in the nucleophilic addition step.

(c) Intramolecular cyclization step

Following the formation of Cat-X-IM2 through the nucleophilic addition process, the O(1) atom of CO_2 is activated by the ChB catalysts, facilitating the O(2) atom of CO_2 intramolecular substitution with the C(1) of Cat-X-IM2. The O(2) atom of CO_2 undergoes rearrangement with the C(1) atom of Cat-X-IM2, triggering the intramolecular cyclization reaction: O(2) forms a bond with C(1) with the departure of the I ion, ultimately yielding the product (i.e. phenylethylene carbonate). According to the Gibbs free energy curves (Figure 2), the energy barriers of the nucleophilic addition step are 11.6, 12.7, 11.8, 14.4, 15.5, 18.3, 21.4, and 19.2 kcal/mol, respectively. From these energy barriers, one can conclude that different ChB catalysts with different kinds of chalcogen atoms can also facilitate the intramolecular cyclization reaction.

3.3 Generalized Kohn–Sham energy decomposition analysis

Quantitative analysis of the interactions between catalysts and substrates can enhance our understanding of the catalytic effects of different types of ChB catalysts. Energy decomposition analysis (EDA) is a powerful theoretical method. Among lots of EDA methods [58-60], the generalized Kohn–Sham energy decomposition analysis (GKS-EDA) scheme has significantly improved the adaptability of DFT functionals [58-59]. The GKS-EDA scheme enables interaction analysis using various DFT functions in both gas-phase and solvent environments. Therefore, the GKS-EDA method is employed in this work for analyzing the interactions between ChB catalysts and the substrates. It is worth mentioning that GKS-EDA decomposes the total interaction free energy (ΔE^{TOT}) into electrostatic (ΔE^{ele}), exchange-repulsion ($\Delta E^{ex\text{-}rep}$), polarization (ΔE^{pol}), correlation (ΔE^{corr}), as shown in Equation (1).

$$\Delta E^{TOT} = \Delta E^{ele} + \Delta E^{ex\text{-}rep} + \Delta E^{pol} + \Delta E^{corr} \quad (1)$$

Figure 4 and Table S1 depict the decomposition of Cat-X-COM1. The computational analysis reveals that the electrostatic term predominates in the catalytic systems for all 8 ChB Catalysts, which are -9.14, -9.61, -10.04, -12.15, -16.50, -18.56, -11.28, and -14.31 kcal/mol, respectively, indicating that the electrostatic effect plays a pivotal role in modulating the strength of ChB between the catalyst and styrene oxide. This electrostatic term induces reorganization of the distribution of electrons for two different fragments, which is potentially accompanied by partial charge transfer between these fragments. The electronic redistribution facilitates the formation of the ChB between the chalcogen atom and the O atom as well as the formation of Cat-X-COM1. Concurrently, the computational investigations demonstrated that the Te-based catalysts exhibited significantly enhanced performance metrics across the evaluated energy components, including ΔE^{ele}, ΔE^{pol}, and ΔE^{TOT}, when systematically compared to the Se-based catalysts.

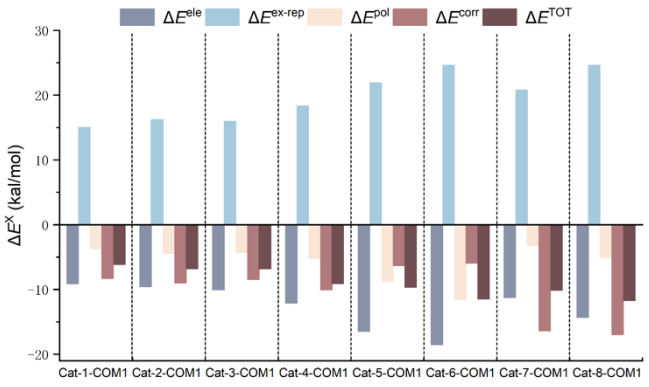

Figure 4. Dissected interactions of free energies (ΔE^{X}, X=ele/ex-rep/pol/ corr/TOT) for Cat-X-COM1.

3.4 Molecular formation density difference analysis

To verify the occurrence of electron transfer during the complex formation process, molecular formation density difference (MFDD) analysis is employed for the Cat-X-COM1 (X=1-8), which validates the catalytic effects of different types of ChB catalysts on the CCE reaction. The regions where electron density decreases are shown in blue (region 1) while the regions where electron density increases are shown in red (region 2) in Figure 5. MFDD results reveal that the chalcogen atoms of the catalysts are located in region 1, while the O atom of styrene oxide is located in region 2. According to the data presented in Table S2, it can be observed that the reduction in electron density is more pronounced for the Te-based catalysts (Cat2, Cat4, Cat6, and Cat8 are -0.0403, -0.0474, -0.0550 and -0.0372 a.u., respectively) compared to the Se-based catalysts (Cat1, Cat3, Cat5, and Cat7 are -0.0288, -0.0301, -0.0440 and -0.0193 a.u., respectively) with same catalysts motifs. This finding suggests that the Te-based catalysts exhibit superior capability in activating the O atom of styrene oxide. The larger electron density reduction associated with the Te-based catalysts implies a stronger interaction with the O atom of styrene oxide, thereby facilitating the activation process. This enhanced capability of activating the reactant of the Te-based catalysts in Cat-X-COM1 may contribute to their good catalytic performance in the CCE reaction.

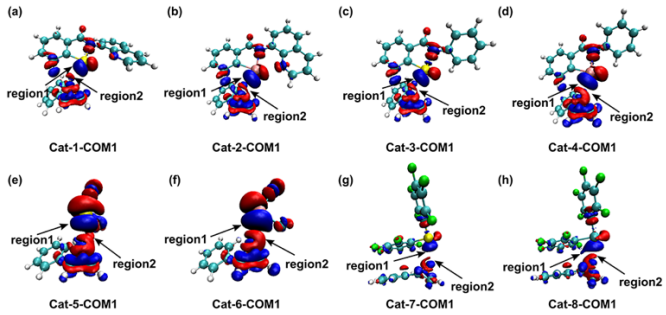

Figure 5. Plots of the computed density differences on the 0.0006 a.u. (electrons/bohr^3) the contour of the electronic density: (a) Cat-1-COM1; (b) Cat-2-COM1; (c) Cat-3-COM1; (d) Cat-4-COM1; (e) Cat-5-COM1; (f) Cat-6-COM1; (g) Cat-7-COM1; and (h) Cat-8-COM1 (region 1: The electron density on the surface of the Se or Te atom in the catalyst; region 2: The electron density on the surface of the O atom in the styrene oxide).

3.5 Quantum theory of atoms in molecules analysis

QTAIM has been demonstrated to play a pivotal role in the investigation of weak interaction. To analyze the interactions between the Se/Te atoms in the catalysts and the O atom in styrene oxide, QTAIM analysis was performed for the Cat-X-COM, which validates the catalytic effects of different types of ChB catalysts on the CCE reaction. Figure S3 displays the molecular graphs of Cat-X-COM. It can be seen that there exist bond critical points (BCPs) between the Se/Te atoms of the eight catalysts and the O atom in styrene oxide, thereby confirming the presence of the Se/Te···O chalcogen bonding.

According to the data presented in Table 1, it can be observed that all the values of the Laplacian $\nabla^2\rho_b$ at the BCPs are greater than zero, which indicates that the interaction belongs to the closed-shell interaction. The electron densities ρ_b of the Cat-X-COM1 range from 0.0122 to 0.0280, respectively. The ρ_b values of the Te-based catalysts (Cat-2, Cat-4, Cat-6 and Cat-8) are higher than the Se-based catalysts (Cat-1, Cat-3, Cat-5 and Cat-7). This indicates that the ChB formed by the Te-based catalysts are stronger than Se-based catalysts, thereby more effectively facilitating the activation process. Furthermore, the $-G_b/V_b$ values of the Cat-1-COM1 to Cat-5-COM1, Cat-7-COM1, and Cat-8-COM1 are all larger than 1.0, indicating that the interactions between the Se/Te atoms in these catalysts and the O atom in styrene oxide are non-covalent interactions. In contrast, the $-G_b/V_b$ values of the Cat-6-COM1 are between 0.5 and 1.0, suggesting that the interactions between the Te atom in the catalyst and the O atom exhibit partial covalent character. Additionally, Cat-6-COM1 displays the highest ρ_b values. These results demonstrate that the interactions between Cat-6 and the O atom in styrene oxide are stronger, leading to a corresponding reduction in the Gibbs free energy barrier for the ring-opening step.

4. Conclusion

In summary, the present work investigates the performance of Se/Te-based ChB catalysts to catalyze the cycloaddition reaction of CO_2 with styrene oxide through DFT calculations. The following conclusions can be drawn:

The catalytic mechanism of ChB catalysts for the cycloaddition reaction of CO_2 with styrene oxide can be divided into three sub-steps: (1) ring-opening step, (2) nucleophilic addition step, and (3) intramolecular cyclization step. The proposed reaction mechanism is expected to enrich the understanding of the role of ChB catalysis in CO_2 conversion.

The selected eight ChB catalysts utilized in this work have shown the potential for catalyzing the CCE reaction from the computational results. Both Se-based and Te-based catalysts have potential for utilization in the reaction, the overall catalytic performance of Te-based catalysts was superior to that of Se-based catalysts.

The most positive electrostatic potentials ($V_{s,\,max}$) of the ChB catalysts and the electrostatic term (ΔE^{ele}) of the ChB binding energies play pivotal roles in the ChB catalysis in the CCE reaction. Furthermore, the electron density at the ChB critical point and the electron density difference also play important roles in the ChB catalysis in the reaction. Cat-5 and Cat-6 have the better catalytic performance among all these eight catalysts because of their stronger electrostatic potentials and ΔE^{ele} terms, which prompted Cat-5 and Cat-6 to form stronger ChB.

This work explores the mechanism of the cycloaddition reaction of CO_2 with styrene oxide catalyzed by ChB catalysts and shows the potential of different chalcogen atoms (i.e. Se and Te) based ChB catalysts. Moreover, this work offers significant guidance for the future development of more efficient catalysts for the cycloaddition of CO_2 into epoxides.

Table 1. Topological Properties of Non-Covalent Interactions at the BCPs of the Complexes (in a.u.).

Complex	ρ_b	$\nabla^2\rho_b$	G_b	V_b	H_b	$-G_b/V_b$
Cat-1-COM1	0.0160	0.0554	0.0127	-0.0116	0.0011	1.0943
Cat-2-COM1	0.0167	0.0512	0.0125	-0.0123	0.0003	1.0212
Cat-3-COM1	0.0169	0.0593	0.0136	-0.0124	0.0012	1.0969
Cat-4-COM1	0.0213	0.0692	0.0170	-0.0167	0.0003	1.0173
Cat-5-COM1	0.0271	0.0918	0.0224	-0.0218	0.0006	1.0265
Cat-6-COM1	0.0280	0.0935	0.0236	-0.0239	-0.0002	0.9900
Cat-7-COM1	0.0122	0.0430	0.0097	-0.0087	0.0010	1.1196
Cat-8-COM1	0.0157	0.0505	0.0122	-0.0117	0.1066	1.0382

Acknowledgements

This work was funded by the Natural Science Foundation of Hebei Province (B2022205022, Y.Z.), the National Natural Science Foundation of China (22303025, W-K.C.), the Science Foundation of Hebei Normal University (L2023B12, W.-K.C.), and the Graduate Innovation Funding Project of Hebei Normal University (XCXZZSS202433, H. Z.).

Supporting Information

The online version contains supplementary material available at website Detailed data of GKS-EDA and MFDD; Cartesian coordinates.
https://global-sci.com/storage/self-storage/cicc-2025-70-1-r1-si.pdf

References

[1] Robidas R., Reinhard D. L., Legault C. Y., Huber S. M. Iodine(iii)-based halogen bond donors: properties and applications. *Chem. Rec.*, **21** (2021), 1912-1927.

[2] Jovanovic D., Poliyodath Mohanan M., Huber S. M. Halogen, chalcogen, pnictogen and tetrel bonding in non-covalent organocatalysis: an update. *Angew. Chem. Int. Ed.*, **63** (2024), e202404823.

[3] Kaasik M., Kanger T. Supramolecular halogen bonds in asymmetric catalysis. *Front. Chem.*, **8** (2020), 599064.

[4] Sekar G., Nair V. V., Zhu J. Chalcogen bonding catalysis. *Chem. Soc. Rev.*, **53** (2024), 586-605.

[5] Pale P., Mamane V. Chalcogen bonding catalysis: tellurium, the last frontier? *Chem. Eur. J.*, **29** (2023), e202302755.

[6] Murray J. S., Lane P., Clark T., Politzer P. σ-hole bonding: molecules containing group vi atoms. *J. Mol. Model.*, **13** (2007), 1033-1038.

[7] Aakeroy C. B., Bryce D. L., Desiraju G. R., Frontera A., Legon A. C., Nicotra F., Rissanen K., Scheiner S., Terraneo G., Metrangolo P., et al. Definition of the chalcogen bond (IUPAC Recommendations 2019). *Pure Appl. Chem.*, **91** (2019), 1889-1892.

[8] Clark T., Hennemann M., Murray J. S., Politzer P. Halogen bonding: the σ-hole. *J. Mol. Model.*, **13** (2006), 291-296.

[9] Benz S., López-Andarias J., Mareda J., Sakai N., Matile S. Catalysis with chalcogen bonds. *Angew. Chem. Int. Ed.*, **56** (2017), 812-815.

[10] Wonner P., Dreger A., Vogel L., Engelage E., Huber S. M. Chalcogen bonding catalysis of a nitro-Michael reaction. *Angew. Chem. Int. Ed.*, **58** (2019), 16923-16927.

[11] Zhang Q. Y., Chan Y. Y., Zhang M. Y., Yeung Y. Y., Ke Z. H. Hypervalent chalcogenonium···π bonding catalysis. *Angew. Chem. Int. Ed.*, **61** (2022), e202208009.

[12] Kong X., Zhou P. P., Wang Y. Chalcogen···π bonding catalysis. *Angew. Chem. Int. Ed.*, **60** (2021), 9395-9400.

[13] Bhanja P., Modak A., Bhaumik A. Supported porous nanomaterials as efficient heterogeneous catalysts for CO_2 fixation reactions. *Chem. Eur. J.*, **24** (2018), 7278-7297.

[14] Pal T. K., De D., Bharadwaj P. K. Metal-organic frameworks as heterogeneous catalysts for the chemical conversion of carbon dioxide. *Fuel*, **320** (2022), 123904.

[15] Truong C. C., Mishra D. K. Catalyst-free fixation of carbon dioxide into value-added chemicals: a review. *Environ. Chem. Lett.*, **19** (2021), 911-940.

[16] Kindermann N., Jose T., Kleij A. W. Synthesis of carbonates from alcohols and CO_2. *Top. Curr. Chem.*, **375** (2017), 15.

[17] Mundo F., Caillol S., Ladmiral V., Meier M. A. R. On sustainability aspects of the synthesis of five-membered cyclic carbonates. *ACS Sustainable Chem. Eng.*, **12** (2024), 6452-6466.

[18] Zou B., Hu C. Halogen-free processes for organic carbonate synthesis from CO_2. *Curr. Opin. Green Sustainable Chem.*, **3** (2017), 11-16.

[19] Guo L., Lamb K. J., North M. Recent developments in organocatalysed transformations of epoxides and carbon dioxide into cyclic carbonates. *Green Chem.*, **23** (2021), 77-118.

[20] Mańka D., Siewniak A. Deep eutectic solvents as catalysts for cyclic carbonate synthesis from CO_2 and epoxides. *Molecules*, **27** (2022), 9006.

[21] Marciniak A. A., Lamb K. J., Ozorio L. P., Mota C. J. A., North M. Heterogeneous catalysts for cyclic carbonate synthesis from carbon dioxide and epoxides. *Curr. Opin. Green Sustainable Chem.*, **26** (2020), 100365.

[22] Lozano P., García-Verdugo E. From green to circular chemistry paved by biocatalysis. *Green Chem.*, **25** (2023), 7041-7057.

[23] Sheldon R. A. Green chemistry and resource efficiency: towards a green economy. *Green Chem.*, **18** (2016), 3180-3183.

[24] Delidovich I., Palkovits R. Catalytic versus stoichiometric reagents as a key concept for green chemistry. *Green Chem.*, **18** (2016), 590-593.

[25] Jain S., Batabyal M., Thorat R. A., Choudhary P., Jha R. K., Kumar S. 2-Benzamide tellurenyl iodides: synthesis and their catalytic role in CO_2 mitigation. *Chem. Eur. J.*, **29** (2023), e202301502.

[26] Zhao Y., Truhlar D. G. The M06 suite of density functionals for main-group thermochemistry, thermochemical kinetics, non-covalent interactions, excited states and transition elements: two new functionals and systematic testing of four

M06-class functionals and 12 other functionals. *Theor. Chem. Acc.*, **120** (2008), 215-241.

[27] Weigend F., Ahlrichs R. Balanced basis sets of split-valence, triple-zeta-valence and quadruple-zeta-valence quality for H to Rn: design and assessment of accuracy. *Phys. Chem. Chem. Phys.*, **7** (2005), 3297-3305.

[28] Zhao Y. C., Chen F. M. Empirical likelihood inference for censored median regression model via non-parametric kernel estimation. *J. Multivariate Anal.*, **99** (2008), 215-231.

[29] Grimme S., Antony J., Ehrlich S., Krieg H. A consistent and accurate *ab initio* parametrization of density-functional dispersion correction (DFT-D) for the 94 elements H–Pu. *J. Chem. Phys.*, **132** (2010), 154104-154122.

[30] Frisch M. J., Trucks G. W., Schlegel H. B., Scuseria G. E., Robb M. A., Cheeseman J. R., et al. *Gaussian 16, Revision C.01.* Gaussian Inc., Wallingford CT, 2019.

[31] Grimme S. Exploration of chemical compound, conformer and reaction space with meta-dynamics simulations based on tight-binding quantum-chemical calculations. *J. Chem. Theory Comput.*, **15** (2019), 2847-2862.

[32] Pracht P., Bohle F., Grimme S. Automated exploration of the low-energy chemical space with fast quantum-chemical methods. *Phys. Chem. Chem. Phys.*, **22** (2020), 7169-7192.

[33] Pracht P., Grimme S., Bannwarth C., Bohle F., Ehlert S., Feldmann G., Gorges J., Müller M., Neudecker T., Plett C., et al. CREST – a program for the exploration of low-energy molecular chemical space. *J. Chem. Phys.*, **160** (2024), 114110.

[34] Tomasi J., Mennucci B., Cammi R. Quantum-mechanical continuum solvation models. *Chem. Rev.*, **105** (2005), 2999-3094.

[35] Talebian E., Talebian M. A general review on the derivation of the Clausius–Mossotti relation. *Optik*, **124** (2013), 2324-2326.

[36] Benatto L., Koehler M. Effects of fluorination on exciton-binding energy and charge transport of π-conjugated donor polymers and the ITIC molecular acceptor: a theoretical study. *J. Phys. Chem. C*, **123** (2019), 6395-6407.

[37] Fukui K. The path of chemical reactions – the IRC approach. *Acc. Chem. Res.*, **14** (1981), 363-368.

[38] Liu S.-C., Zhu X.-R., Liu D.-Y., Fang D.-C. DFT calculations in solution systems: solvation energy, dispersion energy and entropy. *Phys. Chem. Chem. Phys.*, **25** (2023), 913-931.

[39] Zhang J., Lu T. Efficient evaluation of electrostatic potential with computerized optimized code. *Phys. Chem. Chem. Phys.*, **23** (2021), 20323-20328.

[40] Reed A. E., Weinhold F. Natural localized molecular orbitals. *J. Chem. Phys.*, **83** (1985), 1736-1740.

[41] Zheng S., Hada M., Nakatsuji H. Topology of density difference and force analysis. *Theor. Chim. Acta*, **93** (1996), 67-78.

[42] Li W., Zeng Y., Zhang X., Zheng S., Meng L. The enhancing effects of group v σ-hole interactions on the F···O halogen bond. *Phys. Chem. Chem. Phys.*, **16** (2014), 19282-19289.

[43] Roux M., Besnainou S., Daudel R. Recherches sur la répartition de la densité électronique dans les molécules. *J. Chim. Phys. Phys.-Chim. Biol.*, **53** (1956), 218-221.

[44] Lu T., Chen F. W. Multiwfn: a multifunctional wave-function analyser. *J. Comput. Chem.*, **33** (2012), 580-592.

[45] Humphrey A. D. W., Schulten K. VMD: visual molecular dynamics. *J. Mol. Graphics*, **14** (1996), 33-38.

[46] Legault C. Y. *CYLview20.* Université de Sherbrooke, 2020.

[47] Su P. F., Jiang Z., Chen Z. C., Wu W. Energy decomposition scheme based on the generalized Kohn–Sham scheme. *J. Phys. Chem. A*, **118** (2014), 2531-2542.

[48] Su P. F., Tang Z., Wu W. Generalized Kohn–Sham energy decomposition analysis and its applications. *WIREs Comput. Mol. Sci.*, **10** (2020), e1460.

[49] Tang Z., Song Y., Zhang S., Wang W., Xu Y., Wu D., Wu W., Su P. XEDA: a fast and multipurpose energy decomposition analysis program. *J. Comput. Chem.*, **42** (2021), 2341-2351.

[50] Keith T. A. *AIMAll* (version 15.09.27). TK Gristmill Software, Wallingford CT, 2019.

[51] Bader R. F. W. *Atoms in Molecules: A Quantum Theory.* Oxford University Press, Oxford, 1994.

[52] Li S., Xu T., van Mourik T., Früchtl H., Kirk S. R., Jenkins S. Halogen and hydrogen bonding in halogenabenzene/NH_3 complexes compared using next-generation QTAIM. *Molecules*, **24** (2019), 2875-2886.

[53] Li Y., Zhao C., Zhang H. Y., Zeng Y. L. Halogen-bond catalysis of the [4+2] cycloaddition reaction of 2-alkenylindoles: catalytic modes and stereoselectivity. *Phys. Chem. Chem. Phys.*, **26** (2024), 477-484.

[54] Wang W., Li X. X., Zhou P. P., Wang Y. Catalysis with supramolecular carbon-bonding interactions. *Angew. Chem. Int. Ed.*, **60** (2021), 22717-22721.

[55] Boyd R. J. The relative sizes of atoms. *J. Phys. B: At. Mol. Phys.*, **10** (1977), 2283-2291.

[56] Wang Z., Shi B., Zhao C., Zeng Y. Hypervalent chalcogen-bond catalysis on the intramolecular aza-Michael reaction of aminochalcone: catalytic performance and chalcogen bond properties. *Chem. Eur. J.*, **30** (2024), e202401886.

[57] Wang Z., Zhao C., Li X., Shi B., Zeng Y. Neutral monodentate and hypervalent chalcogen-bond catalysis on the intramolecular Rauhut–Currier reaction of bis(enones): a DFT study. *Chem. Eur. J.*, **29** (2023), e202300171.

[58] Khaliullin R. Z., Cobar E. A., Lochan R. C., Bell A. T., Head-Gordon M. Unravelling the origin of intermolecular interactions using absolutely localized molecular orbitals. *J. Phys. Chem. A*, **111** (2007), 8753-8876.

[59] Wu Q., Ayers P. W., Zhang Y. K. Density-based energy decomposition analysis for intermolecular interactions with variationally determined intermediate-state energies. *J. Chem. Phys.*, **131** (2009), 164112-164119.

[60] Glendening E. D., Streitwieser A. Natural energy decomposition analysis: an energy partitioning procedure for molecular interactions with application to weak hydrogen bonding, strong ionic and moderate donor–acceptor interactions. *J. Chem. Phys.*, **100** (1994), 2900-2909.